Modeling the Development of the Human Inner Retinal Vasculature and Investigating Conditions for Retinopathy of Prematurity

Christopher A. Graesser

Department of Architecture, University of Washington

Kristine Simon Shea

DMC, Inc.

Scott David Kelly [1]

Department of Mechanical Engineering and Engineering Science
University of North Carolina at Charlotte

Marialuisa Ruiz

Eugene, OR

Charles F. Simmons

Department of Pediatrics
Cedars-Sinai Medical Center

[1] Corresponding author; `scott@kellyfish.net`

Abstract

The development of the human inner retinal vasculature is a complex process involving a delicate balance between the delivery of oxygen to the developing retina by the growing vessel bed and the production of growth factors by hypoxic retinal cells to stimulate vascular growth. Under normal conditions, vessels proliferate steadily across the retina, keeping pace with the increasing oxygen demands of differentiating retinal cells. Disruptions to this process can lead to unregulated capillary growth and retinal damage, a condition known as retinopathy of prematurity (ROP). We present a mathematical model for the healthy development of the human inner retinal vasculature, comprising a system of coupled partial differential equations encoding relationships among capillary density, retinal cell density and maturity, oxygenation of the retinal tissue, and growth factor concentrations. Taking the view that ROP results from one or more perturbations to healthy conditions, we then alter the model to demonstrate how the model can be used to investigate the development of ROP. Our model illuminates potential correlations between the development of ROP and changes over time in clinically measurable, physiological quantities.

Key words: retinal vascular development, retinopathy of prematurity, physiological modeling and simulation

1 Introduction

1.1 Clinical Risk of Retinopathy of Prematurity

Hypoxia that results from the inadequacy of a premature infant's underdeveloped lungs and heart can be alleviated by the delivery of supplemental oxygen in the neonatal intensive care unit (NICU). Inadequate control of oxygenation in the premature retina, however, increases an infant's susceptibility to retinopathy of prematurity (ROP). ROP is characterized by a halt in the normal growth of the inner retinal vasculature, followed by the uncontrolled proliferation of unstable, tortuous capillary structures in one or more regions of the retina [Foos, 1988]. In its most severe form, ROP can lead to retinal detachment and blindness [Phelps, 2001]. ROP is one of the leading causes of blindness in children in the industrialized world [Institute, 2004]. The rate of ROP is as high as 25% among infants in some NICUs, and subsequent blindness — due primarily to retinal detachment — occurs in 2% of infants afflicted [Vaughn et al., 1999].

1.2 Treatment

The exquisite sensitivity of retinal development to changes in oxygenation presents a challenge to the neonatologist faced with the oxygen demands of a preterm infant [Sinha and Tin, 2003]. Recent studies have shown that restricting levels of supplemental oxygen can reduce the occurrence of ROP [Tin et al., 2002]. Close monitoring to avoid prolonged hyperoxia and fluctuations between hypoxia and hyperoxia have been found to result in an 80% drop in the incidence of ROP [Chow et al., 2003]. The STOP-ROP clinical study found, however, that elevated levels of oxygen delivered after the initiation of ROP may not significantly change the disease outcome [The STOP-ROP Multicenter Study Group, 2000].

Once ROP develops, cryo- or laser surgery can prevent progression to more severe stages in some cases, but recurrence and scarring are common problems [Cryotherapy for Retinopathy of Prematurity Cooperative Group, 2001; Reynolds, 2001; Hutcheson, 2003]. Current clinical practice recognizes the need to limit oxygen delivery to premature infants [Tin et al., 2002; Chow et al., 2003], but there is no standard protocol to guide clinicians in optimizing oxygen delivery rates for reducing the risk of ROP under varied physiological conditions. We propose that a mathematical model representing the development of the retinal vasculature can be used to explore the sensitivities of the biological pathways that contribute to the incidence and progression of ROP. This model can provide the framework for testing different oxygen delivery protocols under different physiological conditions. Thus, it can formalize the optimization of clinical protocols for the administration of supplemental oxygen to premature infants.

1.3 Retinal Vascular Development

Normal development of the retina begins between gestational weeks 16 and 18, when the retina comprises undifferentiated cells perfused with oxygenated blood from the choriocapillaris, a vascular network at the posterior wall of the eyeball [Provis, 2001]. During weeks 18 through 40 (birth), the differentiation of retinal cells begins at the optic disc and progresses outward [Jakobiec, 1982] (Fig. 1), giving rise to photoreceptive rod and cone cells. In the mature retina, high visual acuity is associated with high photoreceptive cell density in the central two-thirds of the retina; cell density decreases nearer the periphery of the retina — the ora serrata — which provides peripheral vision [Rodieck, 1998].

Differentiation begins in pigment epithelium, rods, and cones. This increases

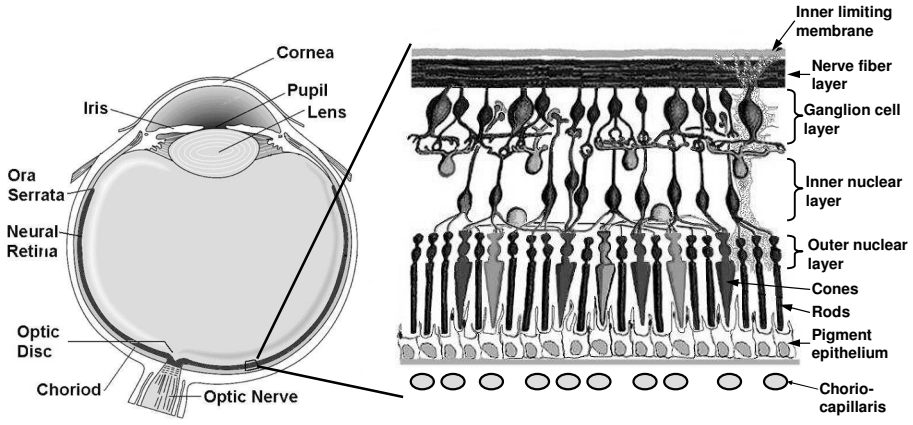

Fig. 1. Retinal anatomy. The fully developed retina, represented on the left by a thick black curve, covers two-thirds of the eye's interior surface. The optic nerve passes through the optic disc to innervate the inner retina. The choriocapillaris nourishes the retina from the posterior wall (choroid). The inner retinal vasculature (not shown) emerges at the optic disc parallel to the optic nerve and radiates outward along the inner surface of the retina to nourish the inner retinal cells. *Inset*: Differentiated retinal cells. Figure modified with permission from [Kolb et al., 2003].

oxygen consumption [Dor et al., 2001], which results in a condition of *physiological hypoxia* in cells farthest from the choriocapillaris, at the inner surface of the retina [Chan-Ling and Stone, 1993]. In response to the lack of oxygen, inner retinal cells secrete vascular endothelial growth factor (VEGF), a chemotactic signal that stimulates and guides capillary growth [Stone et al., 1995; Shima et al., 1995; Dor et al., 2001]. Endothelial cells line every blood vessel; the sprouting of new vessels entails both the spreading out (migration) of existing endothelial cells and the proliferation of new endothelial cells. New capillary growth increases the delivery of oxygen to the retina [Ferrara, 2001; Gerhardt et al., 2003; Dor et al., 2001].

The basement membrane of the outer retina prevents anterior growth of the choriocapillaris towards the inner retina, but the optic nerve penetrates this membrane at the optic disc, providing a passage for new capillary growth. Inner retinal capillaries develop radially from the optic disc along the surface of the inner retina in response to VEGF concentration gradients (Fig. 2(a)). Once differentiating cells receive adequate oxygen, they reduce VEGF secretion, and VEGF levels fall as it is cleared via endocytosis and venous return.

Oxygen diffusion is limited to about 100 microns. As cells farther from the capillary front differentiate, a new ring of VEGF is secreted, begetting a new wave of capillary sprouting and proliferation [Provis, 2001; Gariano, 2001; Hughes et al., 2000]. The advancing wave of vessels typically reaches the ora serrata at 36 (nasal edge) to 40 (temporal edge) weeks gestation [Jakobiec, 1982]. Fig.

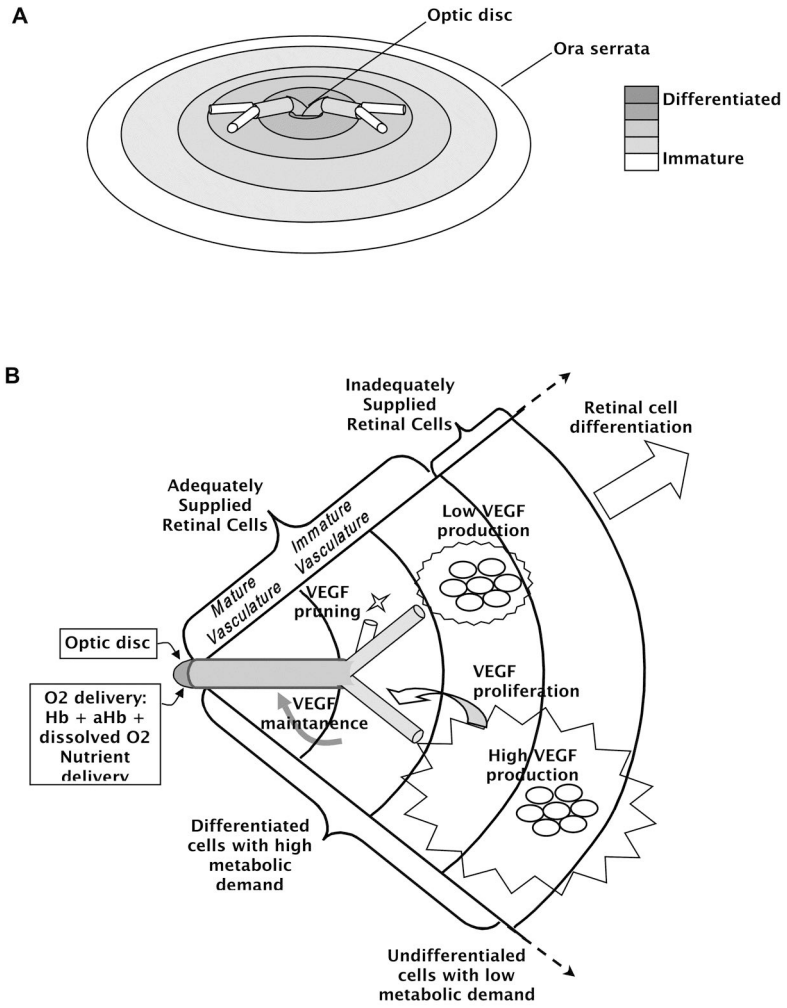

Fig. 2. Retinal Development. (a) The developing retina is represented as a flat disc and regions of differentiating retinal cells are shown as shaded annuli. Capillaries emerge from the optic disc and grow radially on the inner retinal surface, stimulated by growth factors. (b) Simultaneous growth processes are shown in a representative quadrant on the surface of the retina. Hypoxic retinal cells in the outer annulus secrete high levels of VEGF to stimulate capillary proliferation. Adequately nourished retinal cells near the ends of new capillaries secrete reduced levels of VEGF, which results in capillary pruning. After pruning, mature vasculature maintains the nutrient supply to match metabolic demand.

2(b) schematically depicts cellular differentiation and capillary proliferation on the inner retinal surface.

Capillary proliferation is followed by the slower maturation of vessel walls and the production of pericytes, which form a protective outer sheath on mature vessels. Pericytes migrate along the stalks of young blood vessels, forming a single layer of cells that stretches around the vessels, finally encasing them. Initial capillary growth typically exceeds that necessary to meet oxygen

demands; the falling VEGF levels cause atrophy of the immature capillary sprouts in a process called "pruning." The pericyte sheath enclosing a mature vessel renders it resistant to pruning [Benjamin et al., 1998; Risau, 1997; Bergers and Song, 2005]. After pruning, maintenance levels of VEGF ensure the survival of mature vasculature, and the delivery of oxygen matches the needs of retinal cell metabolism.

Note that VEGF is only one of several growth factors that work together to initiate, stimulate, and maintain normal capillary growth and maturation. In developing our model for the regulation of vascular development, however, we have chosen — for the sake of simplicity — to lump the effects of all these growth factors into one group governed by VEGF. We also note that the inner retinal vasculature develops in two branches; one progresses at mid-thickness and the other on the inside surface of the retinal cell layer. Physiologically, these two vascular branches form in parallel paths, with slight differences in timing. For this model, however, we have chosen to treat these capillary branches as a single vessel bed that forms on the inner retinal surface.

1.4 Working Hypothesis for ROP Etiology

There are many perturbations to prenatal development that could initiate unstable retinal capillary growth [Glass, 1998; Phelps, 2001]. One key observation in ROP development is a pause in capillary growth and a ridge of densely packed retinal cells just beyond the halted capillaries. One hypothesis regarding the initiation of ROP suggests that the delivery of supplemental oxygen in the NICU might saturate the developing retina, and stimulate the rapid progression of retinal cellular development in the absence of VEGF secretion. Without VEGF signaling, there is a temporary halt of capillary growth in one or more branches of the capillary network [Phelps, 2001; Hutcheson, 2003]. The high level of supplemental oxygen diffusing out to a 100 micron radius encourages the continued proliferation of retinal cells within a constrained area, causing the cells to form a dense ridge. Under conditions where oxygen perfusion is reduced or no longer sufficient, these cells become hypoxic and begin to secrete high levels of VEGF. The capillaries proliferate rapidly in response, but growth is disorganized. These conditions lead to tortuous capillary growth, reduced vessel wall integrity, and leaky, inefficient nutrient delivery. Leakage from the vasculature and the dense, hypoxic cell layer may disrupt the interstitial matrix and ultimately induce a puckering on the retinal surface that causes the retraction of the retina and detachment from the basement membrane.

1.5 Previous Modeling Work

The mathematical modeling of angiogenesis has received significant attention in other contexts, primarily that of tumor growth. While vascular structure is essentially discrete in nature, several continuous models for the evolution of quantities like mean capillary density appear in the literature. The formation of capillary sprouts from parent vessels exposed to growth factors was previously addressed in [Levine et al., 2000, 2001]. The influence of growth factors and the intracellular matrix (fibronectin) on endothelial cell migration was highlighted in [Chaplain and Anderson, 1997; Anderson and Chaplain, 1998], but the dynamics of growth factor production — critical for our purposes — were not considered therein. Spatial capillary growth in the retina was modeled in [Maggelakis and Savakis, 1996, 1999]. In those studies, a simplified representation of oxygen delivery was implemented, but without regard for changing levels of metabolic activity among retinal cells and without calibration to physiologically realistic parameter values.

Discrete models in the literature typically address the stochastic formation of vascular networks. For example, fractal analysis was applied to the properties of different types of vascular networks in [Gazit et al., 1995] and [Niemisto et al., 2005]. Alternatively, the models in [Anderson and Chaplain, 1998] and [Stokes and Lauffenburger, 1991] were based around the assumption that the motion of an individual endothelial cell governs the motion of the entire capillary sprout to which it is attached. A discrete model for angiogenesis in the cornea was developed in [Tong and Yuan, 2001] assuming sprout formation to exhibit randomness in both the rate and direction of sprout growth. We note that, in the retina, the direction of capillary growth is not random, but is guided by growth factor trails left by glial cells.

Our decision to pursue a continuous model in the present paper reflects, in part, our plans to use our model in developing closed-loop strategies for the time-varying delivery of oxygen in the NICU. Quantitative assessments of developmental states represented in photographic images of neonatal retinas are likely to involve the spatial averaging of local physiological quantities, and the machinery for designing feedback control schemes for systems of PDEs is arguably better developed than that available for discrete systems of the kind in question.

1.6 Scope of the Present Paper

We present a continuous model for the development of the human inner retinal vasculature. This model comprises a system of coupled partial differential

equations encoding relationships among capillary density, retinal cell density and maturity, the partial pressure of oxygen, and growth factor concentration.

Our model incorporates elements absent from the continuous models described above in order to encompass the dynamics of retinal development under both normal conditions and the stressful conditions inherent to prematurity. We parametrize our model to reproduce healthy development, then alter a series of parametric values to demonstrate several characteristics of ROP.

2 Modeling

2.1 Geometry of the Model Domain

The retina can be flattened into an annulus, as shown in Fig. 3. The central boundary of this annulus corresponds to the optic disc and the distal boundary to the ora serrata. The average distance along the retinal surface from the optic disc to the ora serrata (retinal distance) is about 1-2 cm during development, based on eyeball diameters measured in fetuses and infants [Jakobiec, 1982; Galluzzi et al., 2001]. The average thickness of the retina is about 100 μm [Jakobiec, 1982]. This model assigns a retinal distance of 1 cm, representative of early retinal development.

The dark horizontal segment in Fig. 3(b) corresponds to a radial cut through the retina from the optic disc to the ora serrata. Fig. 3(c) depicts this cut edge-on. This slice schematically describes the solution domain of the model. We define x to represent radial distance from the optic disc and y to represent distance through the retina from the choriocapillaris to the inner retinal surface. The retinal cell layer (grey bars) lies between the inner retinal vasculature and the choriocapillaris vasculature (red). Initially, the retinal cell layer is undifferentiated. Differentiation begins at the optic disc (left) and progresses to the ora serrata (right), causing increases in local metabolic activity (darker shading) and oxygen consumption. In the model, the level of differentiation and metabolic demand varies continuously in the radial direction. The rise in oxygen consumption reduces the extent of adequate oxygen perfusion (black and white curves). Oxygen-deficient cells (between the curves) increase their production of VEGF (green). VEGF stimulates the growth of inner retinal capillaries (top red arrow). The capillary front (right point) initially overcompensates with extra sprouting (shading intensity). However, as the hypoxic area moves to the right, the falling VEGF concentration induces subsequent pruning at the trailing end (left). Local metabolic activity, VEGF diffusion, and inner retinal capillary density are calculated along the x axis. Oxygen diffuses from two dynamically distinct sources, and thus requires calculation

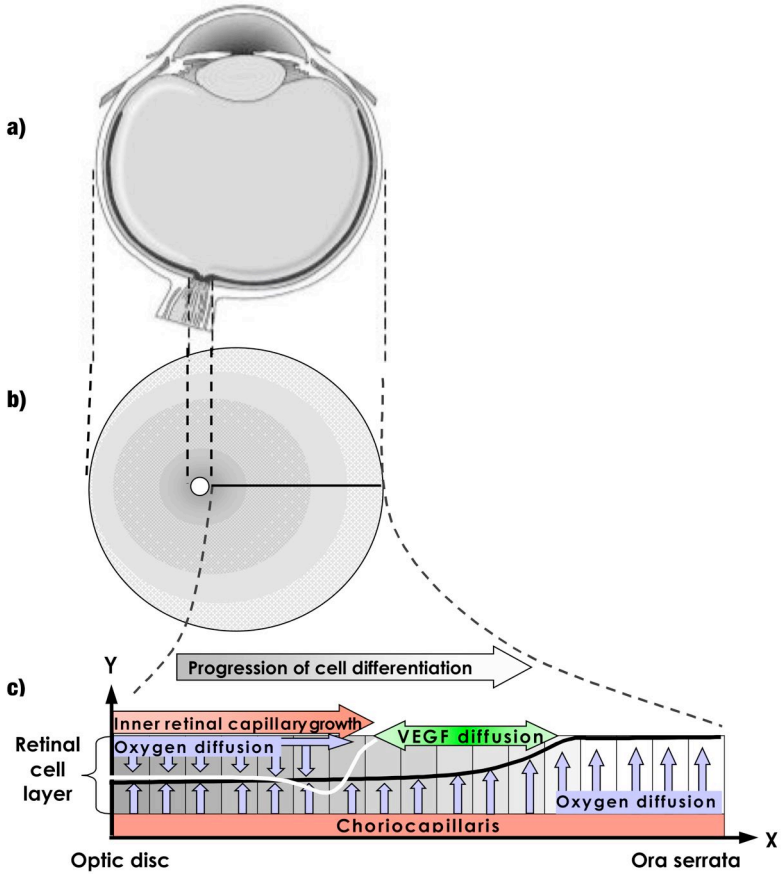

Fig. 3. Flattening the retinal surface. (a) The retina covers 2/3 of the back of the eye (heavy curve). (b) The retina is flattened onto a disc. A radial cut (black line) is made through the thickness of the retina and a side profile is shown in (c). (c) Parameters are defined in a representative section of the developing retina.

in both the x direction and the y direction.

We note that flattening the retina alters the effective values of physical quantities like diffusion rates. In parametrizing our model in Section 3, we assign values to parameters in order to produce the correct behavior of solutions on the flattened domain in Fig. 3(c).

2.2 Assumptions

The model advanced here portrays the physiology underpinning the dynamics of retinal vascular development in terms of four essential quantities, each represented by a time-varying continuous real-valued function on a spatial domain approximating the retinal annulus. The *local metabolic activity* at a spatial point represents a combination of the density and extent of differentiation of local retinal cells. We assume that retinal differentiation, and thus

local metabolic activity, evolves autonomously via a hypothetical signal generated from maturing cells that stimulates differentiation in neighboring cells. Although the factor is hypothetical, it is consistent with paracrine growth factors that have pericellular influence [Hernandez-Sanchez et al., 1995]. The *oxygenation* at a point represents the oxygen availability in retinal tissue resulting from the balance between oxygen delivery and oxygen consumption. Oxygen production is represented in the boundary conditions. We assume that oxygenated blood is well mixed in the heart and distributed equally throughout the arterial circulation. Further, we assume that arterial blood pressure is maintained throughout the circulation. As a result, the oxygen concentration is the same in all retinal capillaries, regardless of distance from the optic disc. These assumptions contribute to the boundary conditions described in Section 2.3.6. The *VEGF concentration* at a point represents a cellular signal generated by oxygen-deficient cells that stimulates capillary growth. Though capillary growth is coordinated by several growth factors, we choose VEGF to represent all growth factors due to the prominent role it plays in retinal vascular development [Ferrara, 2001; Stone et al., 1995]. We further assume that astrocytes ahead of the capillary front on the inner retinal surface are the major producers of VEGF [Provis et al., 1997]; thus, VEGF production is evaluated based on the oxygenation level at the inner retinal surface. The *inner retinal capillary density* at a point represents the vascularity per square millimeter of surface area, and it delivers oxygen to the inner retinal surface, opposite the choriocapillaris. Capillary density varies with VEGF concentration and vascular pruning occurs at low VEGF concentrations (see Section 1).

In modeling the distributions of retinal cells and vessels as spatially continuous functions, we assume the properties of these cells and vessels to be homogeneous over the retinal annulus. For the present paper, we also assume the development of the retina (which proceeds over time from the optic disc to the ora serrata) to be subject only to initial conditions that are radially symmetric about the optic disc. The four quantities introduced above are therefore defined as functions of distance from the optic disc, and not of azimuthal position within the retinal annulus. Moreover, we assume that differentiation occurs uniformly through the thickness of the retina and assign one level of metabolic activity to any given ring (represented as shaded bars in Fig. 3(c)), noting that this value varies continuously in the radial direction. In light of the assumption that astrocytes at the inner retinal surface produce the major VEGF signal and that the retinal metabolic level is homogenous through the thickness of the retina, VEGF diffusion is modeled only in the x direction. This simplification suffices given the homogeneity assumed for the retinal cell layer and the solitary action of VEGF on inner retinal capillary growth. The nascent capillaries are confined to the surface plane and grow in the x direction. We do not include the growth of capillaries within the retinal layer, based on the observation that the medial growth of capillaries shadows the growth pattern

on the surface; therefore, we deem the spatial separation unnecessary for the present model. The oxygenation level is the only quantity considered to vary in both the x and y directions because oxygen diffuses from two mechanistically distinct sources — the choriocapillaris and the inner retinal capillaries.

2.3 Model for Healthy Retinal Development

The following equations describe the evolution of the four components of the model in the healthy state.

2.3.1 Retinal Metabolic Activity

The *local metabolic activity* $r(x,t)$ represents the product of the density of cells and the degree of differentiation at a point in the retina. It is a dimensionless quantity, scaled from 0 to 1. A local metabolic activity of 0 represents no metabolic activity at all. A local metabolic activity of 1 is the maximal metabolic activity allowed in the healthy state; it represents the maximum density of fully differentiated retinal cells.

Our model assumes that retinal differentiation evolves autonomously under healthy conditions, and that metabolic activity changes according to the equation

$$\underset{}{\frac{\partial r}{\partial t}} = \underset{\textit{stimulus}}{D_r \frac{\partial^2 r}{\partial x^2}} + \underset{\textit{metabolic state}}{A_r \left(1 - \frac{r - r_b}{K_r - r_b}\right)(r - r_b)} \,, \tag{1}$$

where the first term (*stimulus*) represents a diffusive signal that stimulates differentiation. Its local concentration depends on the state of cell maturity. This represents a hypothetical signaling factor secreted from neighboring maturing cells, which coordinates concurrent differentiation within a cell layer, consistent with paracrine growth factors [Hernandez-Sanchez et al., 1995]. The second term (*metabolic state*) represents a logistic progression from baseline to the maximum metabolic state. The initial and final distributions of metabolic activity are specified by r_b and K_r, respectively; r_b represents the basal metabolic activity of undifferentiated cells and K_r the metabolic activity of fully differentiated cells. Retinal cell death is not represented in the model at this time.

We assume an initial baseline level of retinal cell density, and therefore metabolic activity; we also assume that retinal cell density is higher near the center of the retina than near the periphery [Rodieck, 1998]. The distribution of maximum metabolic activity K_r is directly proportional to local cell density, and

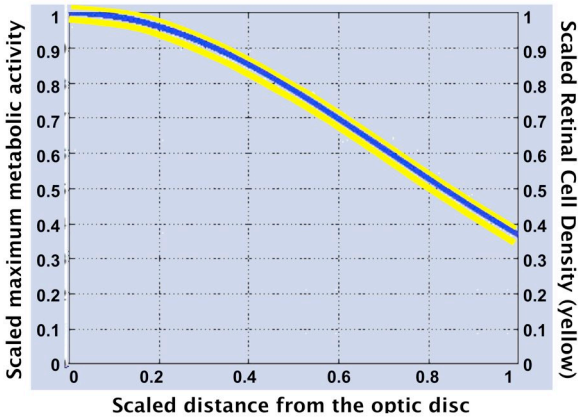

Fig. 4. The distribution of maximum metabolic activity. The maximum metabolic activity distribution (blue line) reflects the approximate cell density distribution (yellow line) in the fully developed healthy retina.

thus varies with distance from the optic disc as

$$K_r(x) = \exp\left(-M_r x^2\right) \ , \tag{2}$$

where the local oxygen consumption M_r reflects the local cell density. This distribution is shown in Fig. 4.

2.3.2 Local Oxygenation Level

The *oxygenation level* at a point represents the oxygen availability in retinal tissue resulting from the balance between oxygen delivery and oxygen consumption. The *oxygenation level* $q(x, y, t)$ varies both radially across the retina and vertically, through its depth, according to the equation

$$\frac{dq}{dt} = D_o \left(\frac{\partial^2 q}{\partial x^2} + \frac{\partial^2 q}{\partial y^2}\right) - M(q, r) \ . \tag{3}$$

diffusion *consumption*

The first term describes oxygen diffusion in both the x (radial) and y (depth) directions because two different sources (the inner retinal circulation and the choriocapillaris) supply oxygen on opposite sides of the retina (note that oxygen production is given by the boundary conditions described in Section 2.3.6). The second term represents oxygen consumption. This equation can be solved analytically, as described in Sections 2.3.6 and 2.3.8. Oxygen deficiency occurs when the result is less than q_{min}, the minimum oxygen required for adequate tissue perfusion. This model for oxygen dynamics, and the solutions we present, represent an elaboration of the approach in [Yu and Cringle, 2001].

Precedents in the literature suggest the use of Michaelis-Menten kinetics to

describe oxygen consumption in the form

$$M(q,r) = B\frac{q}{q_h + q}r \ , \tag{4}$$

where B represents the maximal oxygen consumption rate, q the oxygenation level within retinal tissue, q_h the oxygenation level at half-maximal consumption, and r the local metabolic activity [Beard and Bassingthwaighte, 2001; Kavanagh et al., 2002]. However, this equation is based on conditions *in vitro*, where oxygen fluctuations are more dramatic than conditions *in vivo*, where blood pressure maintains a constant oxygen supply. Thus, we replace the above expression with the simpler expression for oxygen consumption based on local metabolic activity

$$M(q,r) = Br \ . \tag{5}$$

This equation states that oxygen consumption scales directly with metabolic activity. This is appropriate for our model because we assume oxygen deficiency to be a transient phenomenon and exclude conditions in which the lack of oxygen results in cell death.

2.3.3 VEGF Distribution

The *VEGF concentration* $v(x,t)$ varies according to the equation

$$\frac{\partial v}{\partial t} = D_v\frac{\partial^2 v}{\partial x^2} - A_v v - \frac{K_v v}{K_m + v}\delta_{rc}c + f_v(q_m) \ , \tag{6}$$

diffusion *clearance* *production*

an elaboration of an equation appearing in [Maggelakis and Savakis, 1996, 1999].

The first term on the right-hand side is the VEGF diffusion rate. The second and third terms comprise the clearance rate. Clearance is due to VEGF breakdown by proteases ($A_v v$) and the uptake of VEGF through binding and endocytosis by capillary endothelial cells (see below). The fourth term gives the VEGF production rate as a function of the local oxygenation level (q_m).

The clearance due to uptake of VEGF is modeled with Michaelis-Menten binding kinetics. This couples the VEGF concentration to the capillary density $c(x,t)$; the scaling factor δ_{rc} relates the density of capillaries to the concentration of VEGF receptors. The maximal rate of VEGF uptake and the concentration of VEGF at 50% of this rate are represented by K_v and K_m, respectively. The former is proportional to local cell density and its distribution is computed as described for K_r in Fig. 4.

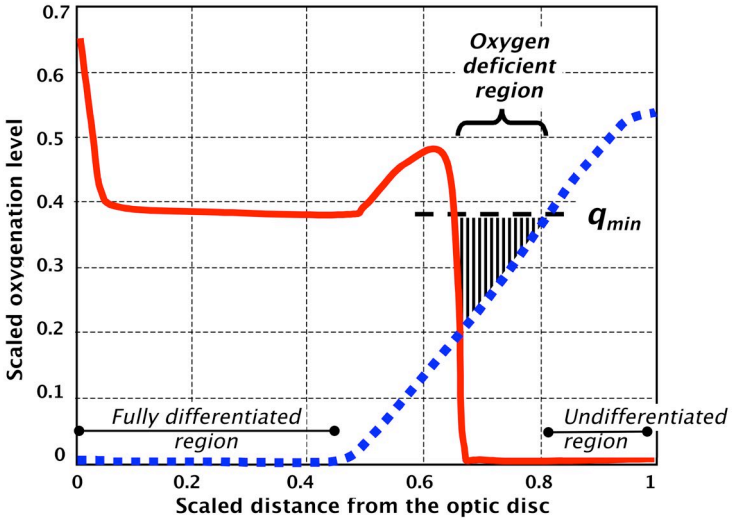

Fig. 5. Oxygen deficiency on the inner retinal surface during development. Oxygen is delivered by the inner retinal capillaries (red solid line) and by the choriocapillaris (blue dotted line). During development, partially differentiated regions (0.5-0.8 from the optic disc) experience local oxygen deficiency when oxygen falls below q_{min} (dashed line). The degree of oxygen deficiency is used to determine the production level of VEGF.

VEGF production by retinal cells $f_v(q_m)$ is driven by the oxygen deficit that occurs when oxygen consumption exceeds oxygen supply, given by

$$f_v(q_m) = \begin{cases} F_v(q_{min} - q_m) & q_m < q_{min} \\ 0 & q_m \geq q_{min} \end{cases}, \tag{7}$$

where q_m is the local oxygenation level and q_{min} is the minimum oxygenation level required for adequate perfusion of retinal cells. The constant F_v relates the oxygenation level to the production of VEGF. Fig. 5 depicts the computation of $f_v(q_m)$.

2.3.4 Inner Retinal Capillary Density

The *inner retinal capillary density* $c(x,t)$, ranging from 0 to 1 in units of $\frac{mm^2\text{capillary}}{mm^2\text{retina}}$, varies across the retina as a function of VEGF signaling and vessel turnover as

$$\underset{elongation}{\frac{\partial c}{\partial t}} = \underset{elongation}{D_c \frac{\partial^2 c}{\partial x^2}} - \underset{chemotaxis}{\frac{\partial}{\partial x}\left(M_v v c \frac{\partial v}{\partial x}\right)} + \underset{turnover}{A_c c}\,. \tag{8}$$

The first term on the right-hand side of the equation represents random motility, which promotes capillary elongation. The second term is based on the chemotactic term in the tumor-induced angiogenesis model of [Anderson and

Chaplain, 1998]; this term represents the VEGF signal that diffuses towards the capillary front. The scalar M_v represents the chemotactic potential [Waltenberger et al., 1994; Wang et al., 2002]. Chemotaxis depends on the number of VEGF receptors available, which is a function of vessel density, and the strength of the VEGF concentration gradient ($\partial v/\partial x$). Capillary growth slows as the capillary front nears the source of VEGF secretion.

The third term on the right-hand side of (8) represents capillary turnover. Capillary stability is dependent on a maintenance level of VEGF [Risau, 1997]; this is represented by the coefficient A_c, given by

$$A_c = \begin{cases} \frac{G_c(v-v_g)}{G_h+(v-v_g)} & v \geq v_g \\ G_d\,(v - v_d) & v \leq v_d \\ 0 & v_d < v < v_g \end{cases}, \tag{9}$$

where the top and middle terms represent capillary growth and decay, respectively. G_v is the maximum capillary proliferation rate. VEGF concentrations above v_g stimulate proliferation and G_h is the concentration that elicits the half-maximal proliferation rate. G_d is the capillary decay rate. To represent vessel "pruning", all vessels are treated as immature; thus, they begin to atrophy (decay) when VEGF falls below the minimum maintenance concentration v_d. For VEGF concentrations between v_d and v_g, the vessel proliferation and decay rates are assumed to be equal, and A_c is set to 0.

We note that representing $c(x,t)$ in units of $\frac{mm^2\text{capillary}}{mm^2\text{retina}}$ will enable the ready comparison of simulation results to measurements of capillary density taken from photographs of infant retinas obtained in the NICU.

2.3.5 Full System of Equations

The complete system of equations describing the development of the healthy inner retinal vasculature is

$$\begin{aligned}
\frac{\partial r}{\partial t} &= \underbrace{D_r \frac{\partial^2 r}{\partial x^2}}_{\text{stimulus}} + \underbrace{A_r \left(1 - \frac{r - r_b}{K_r - r_b}\right)(r - r_b)}_{\text{logistic growth}} \\
\frac{\partial v}{\partial t} &= \underbrace{D_v \frac{\partial^2 v}{\partial x^2}}_{\text{diffusion}} - \underbrace{A_v v}_{\text{decay}} - \underbrace{\frac{K_v v}{K_m + v}\delta_{rc} c}_{\text{uptake}} + \underbrace{\begin{cases} F_v(q_{min} - q_m) & q_m < q_{min} \\ 0 & q_m \geq q_{min} \end{cases}}_{\text{production}} \\
\frac{\partial c}{\partial t} &= \underbrace{D_c \frac{\partial^2 c}{\partial x^2}}_{\text{elongation}} - \underbrace{\frac{\partial}{\partial x}\left(M_v v c \frac{\partial v}{\partial x}\right)}_{\text{chemotaxis}} + \underbrace{\begin{cases} \frac{G_c(v - v_g)}{G_h + v - v_g} c & v \geq v_g \\ G_d\,(v - v_d)\,c & v < v_d \end{cases}}_{\text{growth or decay}} \\
\frac{\partial q}{\partial t} &= \underbrace{D_o \left(\frac{\partial^2 q}{\partial x^2} + \frac{\partial^2 q}{\partial y^2}\right)}_{\text{diffusion}} - \underbrace{Br}_{\text{consumption}} .
\end{aligned} \tag{10}$$

2.3.6 Boundary Conditions

Each of the four PDEs above requires the specification of boundary conditions at both the optic disc ($x = 0$) and the ora serrata ($x = L$). No-flux boundary conditions are given as

$$\frac{\partial r}{\partial x} = \frac{\partial v}{\partial x} = \frac{\partial q}{\partial x} = 0 \qquad (x = 0, x = L) \tag{11}$$

$$\frac{\partial c}{\partial x} = 0 \qquad (x = L)\ . \tag{12}$$

The quantities $r(x,t)$, $v(x,t)$, and $q(x,y,t)$ all change on both boundaries; $c(x,t)$ only changes on the ora serrata. At the optic disc, the inner retinal vessels are considered to "sprout" from existing vessels, and there, the vessel density is fixed as

$$c = c_o \qquad (x = 0)\ . \tag{13}$$

The oxygenation level equation requires additional boundary conditions at the choriocapillaris (y=0) and the inner retinal surface (y=1). For the choriocapillaris boundary, the oxygen is set at a fixed value

$$q = q_c \qquad (y = 0) \tag{14}$$

in view of the relatively constant supply of oxygen in the choriocapillaris circulation q_c. The high rate of blood flow in this region ensures that the amount of oxygen drawn out by the retinal cells will be small compared to the overall supply [Kaufman and Alm, 2003].

The boundary conditions for oxygen at the inner retinal surface depend on the local density of capillaries. When present in sufficient density, the local vessel density and the oxygenation level in the inner retinal circulation determine the boundary condition as

$$q = q_i \frac{c^2}{c_h^2 + c^2} \qquad (y = 1; q_i > 0 \text{ and } c > 0), \tag{15}$$

where q_i is the oxygenation level in the inner retinal capillaries, c is the inner capillary density, and c_h is the half-maximal inner capillary density. The sigmoidal relationship between vessel density and the oxygenation level imposes a minimum level of capillary density for competent oxygen delivery at the inner retinal boundary.

When the inner retinal oxygen delivery drops below a certain level, due to insufficient capillary density or insufficient oxygen content in the blood, more oxygen may be supplied by the choriocapillaris than by the inner retinal circulation. In this case, instead of fixing the concentration, we use a no-flux boundary condition

$$\frac{\partial q}{\partial y} = 0 \qquad (y = 1; q_i = 0, \text{ or } c = 0). \tag{16}$$

The scaled boundary conditions are summarized in Table 1.

2.3.7 Non-Dimensionalized Equations

Simulations are facilitated with a non-dimensionalized, simplified model. We normalize the variable x with respect to L, the distance from the optic disc to the ora serrata, and the variable y with respect to h, the distance from the inner retinal circulation to the choriocapillaris. The retinal differentiation, capillary, VEGF, and oxygen terms are normalized with respect to standard values r_o, c_o, v_o, and q_o, respectively, estimated from the available literature (see Table 2). Finally, time is normalized with respect to a parameter t_c to

Variable	Boundary Location	Boundary Condition
Retinal Differentiation	Ora Serrata	$\frac{\partial r}{\partial x} = 0$
	Optic Disc	$\frac{\partial r}{\partial x} = 0$
VEGF Concentration	Ora Serrata	$\frac{\partial v}{\partial x} = 0$
	Optic Disc	$\frac{\partial v}{\partial x} = 0$
Capillary Density	Ora Serrata	$\frac{\partial c}{\partial x} = 0$
	Optic Disc	$c = 1$
Oxygenation Level	Choriocapillaris	$q = q_c$
	Inner Retina	$q = q_i \frac{c^2}{{c_h}^2 + c^2}$ $\frac{\partial q}{\partial y} = 0$
	Ora Serrata	$\frac{\partial q}{\partial x} = 0$
	Optic Disc	$\frac{\partial q}{\partial x} = 0$

Table 1
Scaled boundary conditions. Recall that the choriocapillaris corresponds to $y = 0$, the inner retina corresponds to $y = 1$, the optic disc corresponds to $x = 0$, and the ora serrata corresponds to $x = 1$.

obtain the scaled equations

$$
\begin{aligned}
\frac{r_o}{t_c}\frac{\partial r^*}{\partial t^*} &= \frac{D_r r_o}{L^2}\left(\frac{\partial^2 r^*}{\partial {x^*}^2}\right) + A_r r_o\left(1 - \frac{r^* - \frac{r_b}{r_o}}{\frac{K_r}{r_o} - \frac{r_b}{r_o}}\right)(r^* - \frac{r_b}{r_o}) \\
\frac{v_o}{t_c}\frac{\partial v^*}{\partial t^*} &= \frac{D_v v_o}{L^2}\left(\frac{\partial^2 v^*}{\partial {x^*}^2}\right) - A_v v_o v^* - K_v \delta_{rc} c_o \frac{v^* c^*}{\frac{K_m}{v_o} + v^*} \\
&\quad + \begin{cases} F_v q_o(\frac{q_{min}}{q_o} - q_m^*) & q_m^* < \frac{q_{min}}{q_o} \\ 0 & q_m^* \geq \frac{q_{min}}{q_o} \end{cases} \\
\frac{c_o}{t_c}\frac{\partial c^*}{\partial t^*} &= \frac{D_c c_o}{L^2}\left(\frac{\partial^2 c^*}{\partial {x^*}^2}\right) - \frac{M_v v_o^2 c_o}{L^2}\left[\frac{\partial}{\partial x^*}\left(v^* c^* \frac{\partial v^*}{\partial x^*}\right)\right] \\
&\quad + \begin{cases} G_c c_o \frac{\left(v^* - \frac{v_g}{v_o}\right)c^*}{\frac{G_h}{v_o} + \left(v^* - \frac{v_g}{v_o}\right)} & v^* \geq \frac{v_g}{v_o} \\ G_d v_o c_o \left(v^* - \frac{v_d}{v_o}\right) c^* & v^* < \frac{v_d}{v_o} \end{cases} \\
\frac{q_o}{t_c}\frac{\partial q^*}{\partial t^*} &= \frac{D_o q_o}{h^2}\left(\frac{h^2}{L^2}\frac{\partial^2 q^*}{\partial {x^*}^2} + \frac{\partial^2 q^*}{\partial {y^*}^2}\right) - B r_o r^* \ .
\end{aligned}
\tag{17}
$$

Here, each variable followed by an asterisk corresponds to the scaled version of that variable; e.g., $c^* = \frac{c}{c_o}$.

Note that the coefficient $\frac{h^2}{L^2}$ appears in the oxygen equation (last equation). However, because $\frac{h^2}{L^2} \ll 1$, it can be neglected. We define one unit of non-dimensional time to be $t_c = \frac{L^2}{M_v v_o^2}$, which corresponds to roughly 10.2 days. Thus, (17) can be simplified to obtain

$$\begin{aligned}
\frac{\partial r}{\partial t} &= d_r \frac{\partial^2 r}{\partial x^2} + \beta \left(1 - \frac{r - r_b}{K_r - r_b}\right)(r - r_b) \\
\frac{\partial v}{\partial t} &= d_v \frac{\partial^2 v}{\partial x^2} - \sigma v - \eta \frac{vc}{\gamma_1 + v} + \begin{cases} \lambda \left(\frac{q_{min}}{q_o} - q_m\right) & q_m < \frac{q_{min}}{q_o} \\ 0 & q_m \geq \frac{q_{min}}{q_o} \end{cases} \\
\frac{\partial c}{\partial t} &= d_c \frac{\partial^2 c}{\partial x^2} - \frac{\partial}{\partial x}\left(vc \frac{\partial v}{\partial x}\right) + \begin{cases} \psi \frac{c\left(v - \frac{v_g}{v_o}\right)}{\gamma_2 + \left(v - \frac{v_g}{v_o}\right)} & v \geq \frac{v_g}{v_o} \\ \omega \left(v - \frac{v_d}{v_o}\right) c & v < \frac{v_d}{v_o} \end{cases} \\
\frac{\partial q}{\partial t} &= d_o \frac{\partial^2 q}{\partial y^2} - \alpha_1 r \ ,
\end{aligned} \tag{18}$$

where

$$d_r = \tfrac{D_r}{M_v v_o^2} \ , \ d_v = \tfrac{D_v}{M_v v_o^2} \ , \ d_c = \tfrac{D_c}{M_v v_o^2} \ , \ d_o = \tfrac{D_o L^2}{M_v v_o^2 h^2} \ , \ \beta = \tfrac{A_r L^2}{M_v v_o^2} \ ,$$

$$\sigma = \tfrac{A_v L^2}{M_v v_o^2} \ , \ \eta = \tfrac{L^2 K_v \delta_{rc} c_o}{M_v v_o^3} \ , \ \lambda = \tfrac{L^2 F_v q_o}{M_v v_o^3} \ , \quad \psi = \tfrac{L^2 G_c}{M_v v_o^2} \ ,$$

$$\omega = \tfrac{L^2 G_d}{M_v v_o} \ , \quad \gamma_1 = \tfrac{K_m}{v_o} \quad , \quad \gamma_2 = \tfrac{G_h}{v_o} \quad , \ \alpha_1 = \tfrac{D_o L^2 B}{M_v v_o^2 q_o} \ ,$$

and the *s have been dropped for notational simplicity.

2.3.8 Solution for the Oxygen Equation

The oxygenation level changes much more rapidly than capillary density, so the distribution of oxygen can be approximated by its equilibrium value on the time scale of capillary growth. Dividing the oxygen equation by d_o and eliminating the derivative with respect to time yields

$$\frac{\partial^2 q}{\partial y^2} = \alpha_2 r \ , \tag{19}$$

where $\alpha_2 = \frac{Bh^2}{D_o q_o}$. This ordinary differential equation can be solved for $q(y,t)$ using the boundary conditions of the model domain.

There are two possible boundary conditions at the inner retina based on the presence or absence of adequate inner capillary density to fix the oxygenation level at the inner retinal surface. This yields two solutions to the oxygenation level equation. The first solution pertains to high inner capillary density,

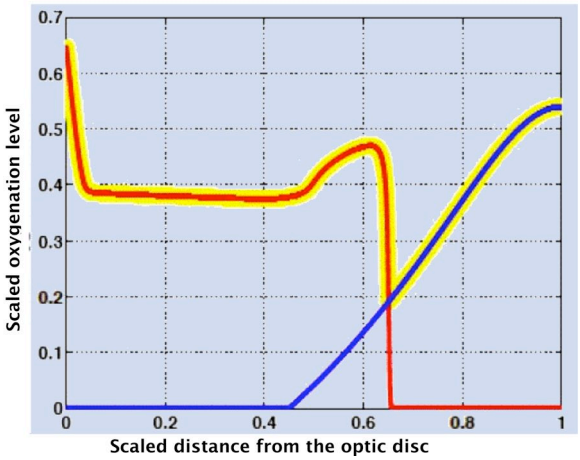

Fig. 6. Concentration of oxygen at the inner retinal surface The curves represent oxygen diffusing from the inner retinal capillaries (red) and oxygen diffusing to the surface from the choriocapillaris (blue). The wide superimposed curve (yellow) represents the combined solution for oxygen levels along the entire retinal surface.

sufficient to fix the oxygenation level:

$$q = \frac{\alpha_2 r}{2} y^2 + \left(\frac{q_i}{q_o} \frac{c^2}{\left(\frac{c_h}{c_o}\right)^2 + c^2} - \frac{\alpha_2 r}{2} - \frac{q_c}{q_o} \right) y + \frac{q_c}{q_o} \ . \tag{20}$$

The second solution pertains to low inner capillary density, insufficient to fix the oxygenation level:

$$q = \frac{\alpha_2 r}{2} y^2 - \alpha_2 r y + \frac{q_c}{q_o} \ . \tag{21}$$

Here oxygen diffusion from the choriocapillaris plays a larger role.

Equations (20) and (21) are evaluated at y=1 for the inner retinal surface; in simulations, the model selects the larger value between

$$\begin{aligned} q|_{y=1} &= \frac{q_i}{q_o} \frac{c^2}{\left(\frac{c_h}{c_o}\right)^2 + c^2} \\ q|_{y=1} &= \frac{q_c}{q_o} - \frac{\alpha_2 r}{2} \end{aligned} \tag{22}$$

for the local oxygenation level q_m (Fig. 6).

Variable	Value	Units	Source
L	9.8	mm	[Jakobiec, 1982]
H	0.13	mm	[Jakobiec, 1982]
D_r	1.56×10^{-3}	$\frac{\text{mm}}{\text{hour}}$	–
A_r	5.83×10^{-3}	$\frac{1}{\text{hour}}$	–
M_r	1.24	–	–
r_b	0.1	–	–
D_v	2.57×10^{-3}	$\frac{\text{mm}}{\text{hour}}$	–
A_v	3.89×10^{-4}	$\frac{1}{\text{hour}}$	–
K_v	10000	$\frac{1}{\text{hour}}$	[Kendall et al., 1999]
K_m	0.7	$\frac{\mu\text{mol}}{\text{mL}}$	[Waltenberger et al., 1994; Wang et al., 2002]
δ_{rc}	1.98×10^{-7}	$\frac{\mu\text{mol mm ret}}{\text{mm cap mL}}$	–
F_v	1.17×10^{-5}	$\frac{\mu\text{mol}}{\text{mL hour mmHg}}$	–
v_o	0.3	$\frac{\mu\text{mol}}{\text{mL}}$	[Lashkari et al., 2000]
D_c	3.94×10^{-5}	$\frac{\text{mm}}{\text{hour}}$	–
M_v	4.38	$\frac{\text{mm}^2}{\text{hour}(\mu\text{mol/mL})^2}$	[Waltenberger et al., 1994; Wang et al., 2002]
G_c	0.093	$\frac{1}{\text{hour}}$	-
G_h	0.7	$\frac{\mu\text{mol}}{\text{mL}}$	–
G_d	0.389	$\frac{\text{mm cap mL}}{\text{mm ret } \mu\text{mol hour}}$	–
c_o	1	$\frac{\text{mm cap}}{\text{mm ret}}$	–
v_g	0.03	$\frac{\mu\text{mol}}{\text{mL}}$	–
v_d	0.01	$\frac{\mu\text{mol}}{\text{mL}}$	–
B	11.11	$\frac{\text{mmHg}}{\text{sec}}$	[Cringle and Yu, 2001]
D_o	.001	$\frac{\text{mm}}{\text{hour}}$	-
q_o	100	mmHg	–
q_i	70	mmHg	–
q_c	70	mmHg	–
q_{min}	40	mmHg	–
c_h	0.4	$\frac{\text{mm cap}}{\text{mm ret}}$	–

Table 2
Model parameter values for the healthy developing retina

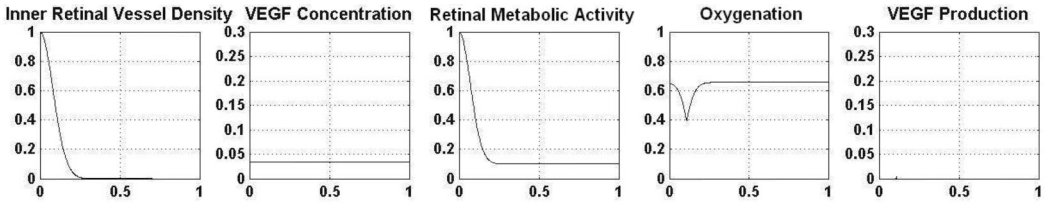

Fig. 7. Initial conditions. Time: 18 weeks gestation, 0 days into simulation, all parameters are evaluated at y=1. The horizontal axis represents the scaled distance x from the optic disc to the ora serrata and the vertical axis represents the non-dimensionalized quantity indicated above each plot.

3 Simulation of Healthy Retinal Development

The simulation described in this section begins when retinal differentiation commences, at about 18 weeks gestation. It represents development on the nasal side of the retina, where the capillaries reach the ora serrata at around 36 weeks gestation.

Direct estimates for seven parameters were obtained from published experimental results, cited in Table 2. The remaining parameter values were derived from values ascribed to analogous physiological parameters in the experimental literature, subject to the constraint that derived parameter values should agree with cited parameter values in their orders of magnitude.

The initial conditions for the simulations were set at

$$\begin{aligned} c_o &= C_o \exp\left(-75x^2\right) \\ v_o &= \frac{v_g - v_d}{2v_o} \\ r_o &= (K_r - r_b)\exp\left(-100x^2\right) + r_b \ . \end{aligned} \tag{23}$$

Fig. 7 shows the beginning of retinal development (18 weeks gestation). Here, vessel density is high only near the optic disc (x=0), where angiogenesis begins. VEGF concentrations are nominal, because there is no oxygen deficiency. Retinal metabolism is high near the optic disc, where retinal cells have begun to differentiate. The oxygenation is sufficient for these cells due to the high vessel density at the optic disc. Slightly farther from the optic disc, oxygen drops because retinal cells have differentiated just beyond the capillary front, and oxygen consumption exceeds oxygen delivery. This low oxygen level triggers the small, corresponding peak in VEGF production. Farther out from the optic disc, towards the ora serrata (x=1), the low metabolic activity of undifferentiated cells is supported by oxygen from the choriocapillaris.

Over time, these features move to the right, as cell differentiation progresses

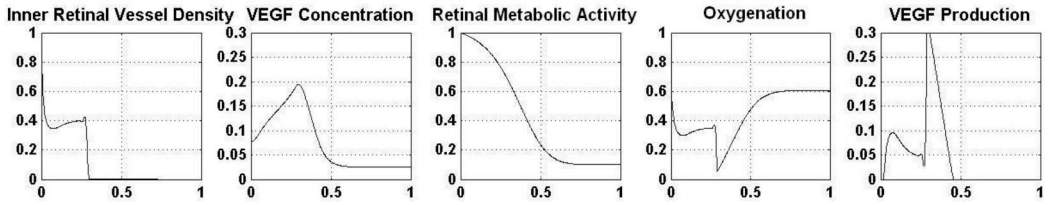

Fig. 8. Time: 22.5 weeks gestation, 31.5 days into simulation.

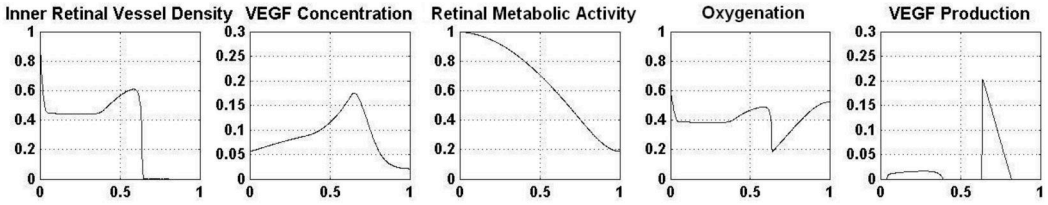

Fig. 9. Time: 27 weeks gestation, 63 days into simulation.

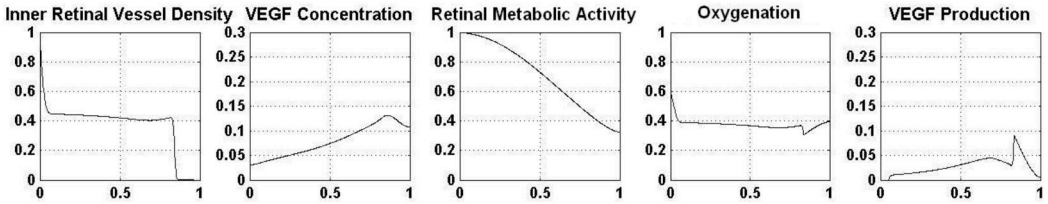

Fig. 10. Time: 31.5 weeks gestation, 94.5 days into simulation.

and capillary growth follows. Figs. 8, 9, and 10 show retinal development at 22.5, 27, and 31.5 weeks gestation, respectively. The central panels of these figures show that the retinal metabolic activity increases over time; thus oxygen consumption rises. This drives down the oxygen availability; the nadirs in the oxygenation panels indicate the regions of oxygen deficiency. The response is an increase in VEGF production (right panels) and, consequently, VEGF concentration (second panels from the left). As expected, the oxygenation nadirs and the VEGF production peaks are aligned just in front of the leading edge of capillary advancement (inner retinal vessel density; left panels).

In Figures 8 and 9, the vessel density panels show a peak in capillary density, coincident with the peak in VEGF concentration. This peak at the leading edge of the capillary front mimics behavior observed in the developing retina. It represents excessive vessel growth in response to the high VEGF concentrations produced to counteract dangerously low oxygen levels. To the left of the peak (closer to the optic disc), retinal cells have matured, and VEGF concentrations have dropped to maintenance levels; here, the trailing vessel density represents vessel "pruning", where excess capillaries are removed. Thus, the vessel density is pruned to meet the metabolic demands of fully differentiated retinal cells. By 31.5 weeks' gestation (Fig. 10), the capillaries have nearly reached the ora serrata. Here, the cell density is lower, with lower oxygen consumption; now, the choriocapillaris is better able to supply sufficient oxy-

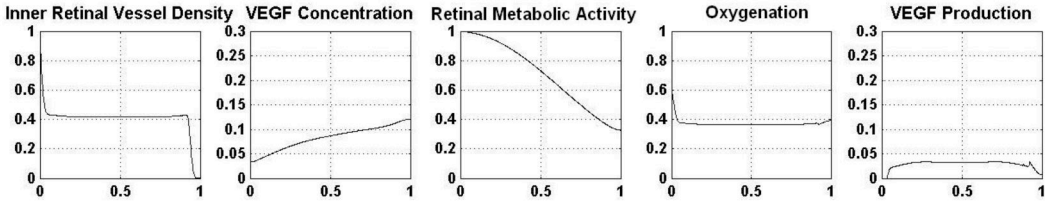

Fig. 11. Time: 36 weeks' gestation, 126 days into simulation.

gen. Therefore, the VEGF production decreases, and the local peak in vessel density almost disappears.

By 36 weeks gestation (Fig. 11), the capillaries approach the ora serrata. They stop advancing, because the low density of retinal cells in the periphery of the retina [Rodieck, 1998] are within reach of oxygen diffusion. The oxygenation level matches the metabolic demands of the fully differentiated retinal cells, and VEGF production falls to maintenance levels.

4 Investigating Conditions for Retinopathy of Prematurity

We next investigate conditions that may contribute to the development of ROP. To that end, we alter some parameters in the above model for healthy retinal development to represent either physiological perturbations or genetic variations. These include changes in oxygen levels, growth constants, and oxygen consumption, described below. In addition, we introduce new parameters to the model to accommodate non-physiological conditions.

4.1 Preliminary Assumptions

We assume that the premature infant was delivered at 24 weeks gestation and immediately exposed to supplemental oxygen. We also assume that when supplemental oxygen was removed, the infant was exposed to ambient oxygen levels, and the heart and lungs functioned normally.

4.1.1 Hypothesis Implementation

An important indicator of ROP is a pause in capillary growth, accompanied by the formation of a hyperplastic ridge [Phelps, 2001; Hutcheson, 2003]. This ridge comprises mainly retinal cells and mesenchymal cells [Mikaniki et al., 2012; Sun et al., 2010], and it is thought to form by retinal cell accumulation due to at least two hypothetical mechanisms [Mikaniki et al., 2012; Sapieha et al., 2010]. First, supplemental oxygen causes hyperoxygenation, and normal

constraints on retinal cell proliferation are thought to be overwhelmed; this could lead to the proliferation and accumulation of retinal cells. Second, oxygen toxicity can cause abnormal activation of growth factors, which may cause a fraction of the dividing endothelial cells to differentiate into mesenchymal cells [Garner, 1985; Deissler et al., 2006].

To implement these mechanisms of retinal cell accumulation in the model, we add two factors to the retinal cell metabolic profile K_r (2). These new factors represent conditional increases in retinal cell number, as follows:

$$K_r(x) = \exp\left(-M_r x^2\right) + \begin{cases} q_1 & q_m > Q_{cr} \\ 0 & q_m < Q_{cr} \end{cases} + \begin{cases} c_1 c & c > C_{cr} \\ 0 & c < C_{cr} \end{cases} . \tag{24}$$

The first term on the right represents the healthy profile, as described in Section 2.3.1. The two new terms thereafter introduce conditional responses to high oxygenation and high capillary density. When local oxygenation q_m exceeds a critical level Q_{cr} at the inner retinal surface, the model constraints on proliferation are altered to raise the maximum metabolic activity (K_r) by a fixed amount q_1. Similarly, when capillary density c exceeds a critical C_{cr} value, a fraction (c_1) of capillary endothelial cells differentiate into retinal cells, and the maximum retinal cell metabolic activity increases by $c_1 c$.

During this hyperoxic interval, we hypothesize that VEGF levels become very low, and the capillaries cease to advance, which causes a "pause" in growth. In fact, we assume that the very low VEGF levels might also trigger capillary pruning, which normally accompanies capillary maturation. In the model, this pruning is controlled by the capillary decay term A_c in (9). However, we assume that the fraction of endothelial cells that converted to retinal cells would no longer be susceptible to pruning. Accordingly, we add a new term, $\exp(-2K_c)$, to the non-dimesionalized decay term in (18) as follows:

$$\text{capillary decay} = \exp(-2K_c)\omega\left(v - \frac{v_d}{v_o}\right)c \quad v < \frac{v_d}{v_o} ; \tag{25}$$

$$K_c = \int_0^t \frac{\max(c - C_{cr}, 0)}{c - C_{cr} + \epsilon} d\tau . \tag{26}$$

Here, K_c increases with time when the capillary density exceeds C_{cr}, but goes to zero when capillary density recedes back to C_{cr}, and ϵ is a small constant to prevent K_c from becoming singular when $c = C_{cr}$.

Upon withdrawal of supplemental oxygen, it is thought that ambient oxygen is insufficient to support the large population of retinal cells. This elicits a dramatic increase in VEGF secretion from hypoxic cells to promote capillary proliferation. In response, endothelial cells rapidly proliferate; however, due to the flood of VEGF [Sonmez et al., 2008; Drake and Little, 1995; Miquerol

et al., 2000] and potential extracellular matrix damage [Sapieha et al., 2010], these endothelial cells cannot elongate in the normal fashion. Furthermore, hypoxic conditions can foster processes that damage the chemotactic trail secreted by astrocytes [Zhang et al., 2011]. Thus, we hypothesize that the rising VEGF concentration and a compromised chemotactic trail combine to cause disorganized capillary growth. Accordingly, we express this by adding a conditional function to the capillary chemotaxis term, as follows:

$$\text{chemotaxis} = \begin{cases} \frac{\partial}{\partial x}\left(vc\frac{\partial v}{\partial x}\right) & c \leq C_{cr} \\ h_1\frac{\partial}{\partial x}\left(vc\frac{\partial v}{\partial x}\right) & c > C_{cr} \end{cases} . \tag{27}$$

Here, the top term in the bracket is the chemotaxis term from (18). It represents capillary chemotaxis in response to VEGF under healthy conditions. The bottom term invokes a reduced chemotactic response when capillary density c exceeds C_{cr}. The new factor h_1 significantly inhibits chemotaxis. Thus, capillaries continue to elongate, but with reduced chemotaxis; consequently, they bunch together and fail to spread out in a regular pattern. This disorganized growth is representative of enlarged, tortuous vessels.

This rendition of capillary formation does not include the fraction of cells that were converted to retinal cells, because they no longer contribute to capillary growth. To prevent possible aberrant model behavior in the initial conditions, this change is introduced only during the second half of the simulation period.

The values for the new parameters (Table 3) were determined empirically in model simulations, because, to our knowledge, no physiological studies have quantifed these parameters. Note that these adjustments to the model do not significantly change the simulation results obtained under the conditions of normal retinal development discussed in Section 3.

Variable	Value
q_1	.5
Q_{cr}	.62
c_1	.001
C_{cr}	.6
h_1	.001
ϵ	-1×10^{-5}

Table 3
Scaled constants used in ROP simulation.

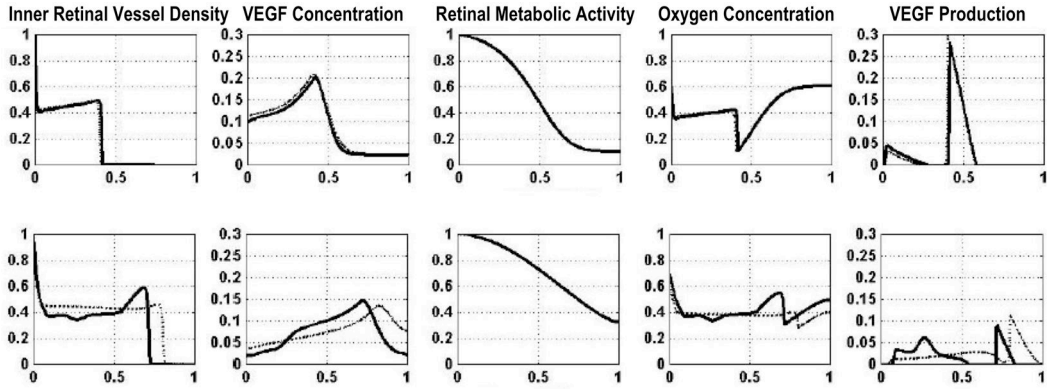

Fig. 12. Simulations before and after short exposure to hyperoxia. (Top) 24 weeks, at birth. (Bottom) 30 weeks, after 2 weeks hyperoxia + 4 weeks room air. Dark lines show simulation after hyperoxic conditions; light lines show simulation under healthy conditions, for comparison.

4.2 Effects of Supplemental Oxygen

The length of time that supplemental oxygen is provided may be an important factor in ROP progression. Few studies have addressed this point, and results have been inconclusive [Askie and Henderson-Smart, 2001]. However, because this is a clinically relevant issue, we demonstrate how the model might be used to guide that type of investigation. Here, we investigate the model's response to oxygen delivery for short or long time periods. In these simulations, we assume normal retinal differentiation until premature delivery (24 weeks). Then, supplemental oxygen is given for either 2 weeks (short exposure) or 6 weeks (long exposure). Subsequently, supplemental oxygen is abruptly removed, and we assume the infant to breathe room air with normal respiration.

4.2.1 Short Exposure to Hyperoxia

In this simulation, after premature birth (24 weeks gestation), supplemental oxygen is given for 15 days (2 weeks), followed by respiration in room air for 4 weeks. Fig. 12 shows results at birth and 6 weeks later.

Fig. 12 shows that the model simulation displays the expected features of ROP. At birth (24 weeks), the simulation shows normal development. At 30 weeks, the short exposure and subsequent withdrawal of supplemental oxygen induces hyper-proliferation of capillaries, as shown by the peak in inner retinal vessel density. However, due to the lack of coherent chemotactic signals, the capillary front does not advance as much as expected under healthy conditions (compare dark and light lines). This results in a highly dense capillary front.

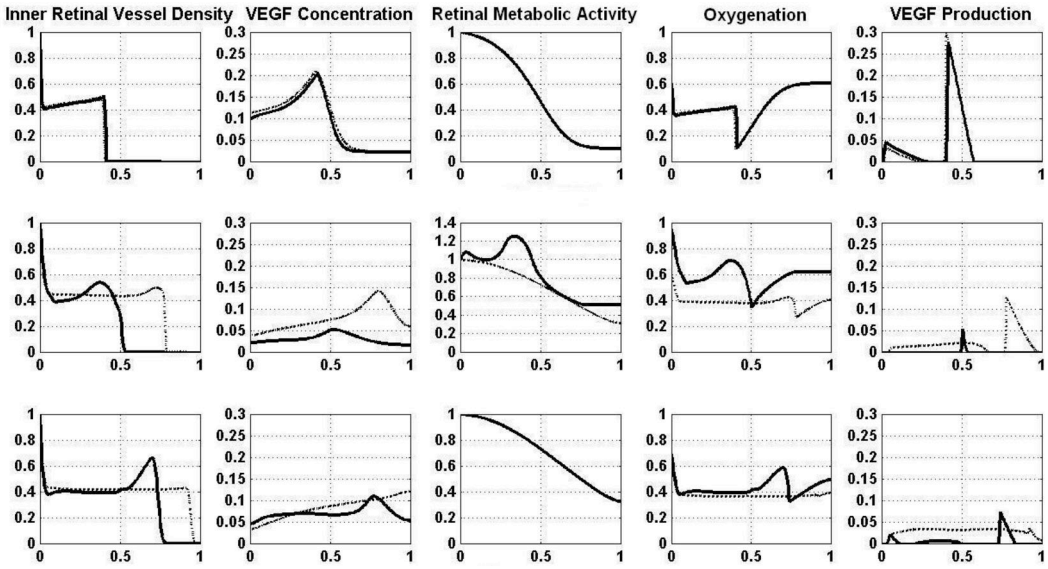

Fig. 13. Simulation results before and after long-term exposure to hyperoxia. (Top) 24 weeks, at birth. (Middle) After 41 days of supplemental oxygen; inner retinal vessel density shows capillary growth has paused, and retinal metabolic activity indicates a ridge of retinal cells. (Bottom) 36 weeks; after 6 weeks hyperoxia + 6 weeks room air. Dark lines show simulation after hyperoxic conditions; light lines show simulation under healthy conditions, for comparison.

4.2.2 Long Exposure to Hyperoxia

In this simulation, supplemental oxygen is given for 41 days (6 weeks) after birth. Fig. 13 shows the results at birth (24 weeks gestation), after supplemental oxygen is withdrawn (30 weeks), and six weeks later.

Figure 13 shows that the model simulation displays more severe features of ROP. At the time supplemental oxygen is withdrawn (middle row), the inner retinal vessel density displays a lag in capillary extension, due to the low VEGF concentrations. Simultaneously, local retinal metabolic activity is distinctly elevated (note the different scale in the center panel, middle row), indicating the formation of a ridge of retinal cells. Six weeks after the withdrawal of supplemental oxygen (bottom row), the capillaries have hyper-proliferated in response to the abrupt increase in VEGF concentration. As described in Section 4.2.1, capillary growth has accumulated in one place due to the reduced chemotactic signaling.

4.3 Genetic Variations

Genetic variations may lead to differential susceptibilities to ROP. The following sections investigate the potential effects of genetic variations on retinal development in premature infants. We vary either the capillary growth con-

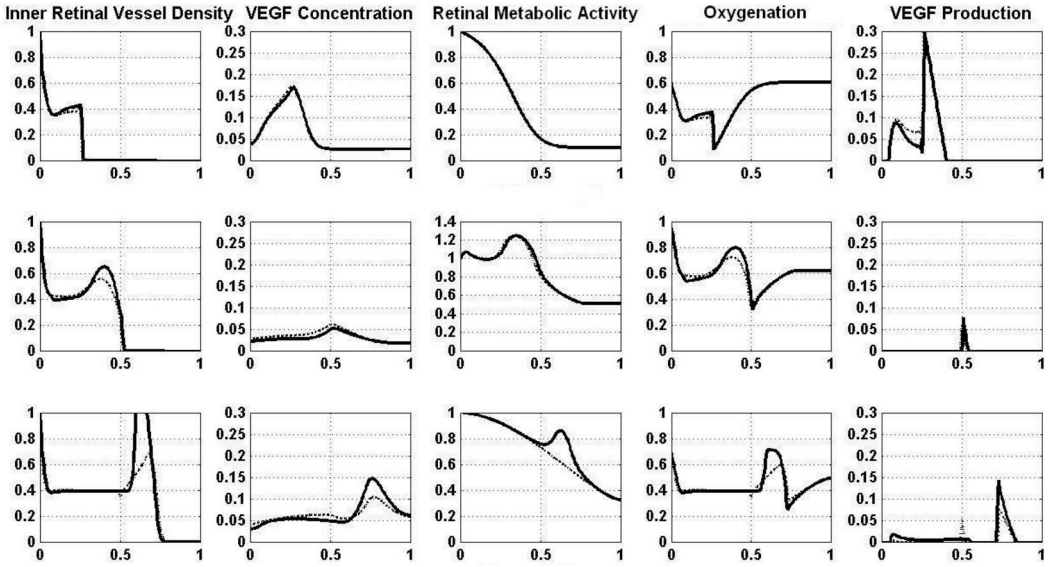

Fig. 14. Simulation results before and after 4 $\frac{1}{2}$ weeks of oxygen exposure with high basal capillary proliferation ($2 \times G_c$). (Top) 24 weeks, at birth. (Middle) After 33 days of supplemental oxygen (28 $\frac{1}{2}$ weeks). (Bottom) After seven subsequent weeks of normal respiration. Dark and light curves correspond to increased and normal basal G_c, respectively, under identical oxygen conditions.

stant or the maximal oxygen consumption rate to represent potential genetic variations. To our knowledge, the range of genetic variation in these parameters among premature infants is unknown. Therefore, we select variations observed under *in vitro* experimental conditions, when available (e.g., [Banin et al., 2006]), and ensure they are sufficiently large to induce a detectable effect.

4.3.1 Increased/Decreased Capillary Growth Constant

To investigate whether the rate of capillary turnover can impact susceptibility to ROP, the capillary growth constant G_c is either doubled or halved. In each simulation, supplemental oxygen is started at birth, continued for $4\frac{1}{2}$ weeks (33 days), then removed abruptly.

Fig. 14 shows the model response to supplemental oxygen application and withdrawal when G_c is doubled. This genetic variant was expected to exhibit reduced capillary turnover, because capillary proliferation should outpace decay. The simulation indicates that, at birth, capillary growth is only slightly more aggressive than normal, due to the pruning signal induced by low VEGF levels. However, after exposure to supplemental oxygen, a larger capillary front is observed in the genetically altered condition compared to the normal genetic condition (light lines). This is because, in both cases, capillary extension pauses without a coherent chemotactic signal, but capillary proliferation con-

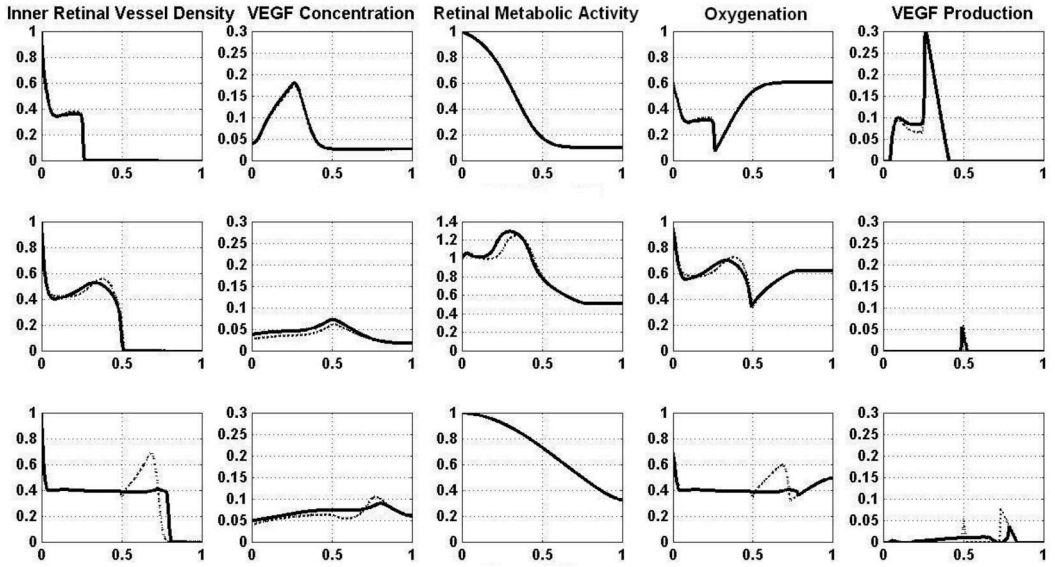

Fig. 15. Simulation results before and after 4 $\frac{1}{2}$ weeks of oxygen exposure in an infant with low basal capillary proliferation ($G_c/2$). (Top) 24 weeks, at birth. (Middle) After 33 days of supplemental oxygen (28 $\frac{1}{2}$ weeks). (Bottom) after seven subsequent weeks of normal respiration (35 $\frac{1}{2}$ weeks). The dark and light curves correspond to reduced and normal basal G_c, respectively, under the same oxygen conditions.

tinues. After oxygen withdrawal and seven weeks of normal respiration, VEGF levels are elevated and capillary density increases dramatically in the altered compared to the normal genetic condition. This suggests that enhanced growth or reduced capillary turnover may confer increased susceptibility to ROP.

Fig. 15 shows the model response when G_c is halved, which was expected to result in an increased capillary turnover rate. The simulation shows that, at birth, capillary growth is normal. After exposure to supplemental oxygen, growth is slightly more retarded in the genetically altered condition compared to the normal genetic condition (light lines). After seven weeks of normal respiration, capillary growth is maintained at a steady level. This suggests that slow growth or increased capillary turnover may confer reduced susceptibility to ROP.

4.3.2 Increased/Decreased Oxygen Consumption Rate

To investigate whether ROP development can be influenced by variations in retinal metabolism, the maximal oxygen consumption rate B is increased or decreased by 15%. In each simulation, supplemental oxygen is given for 33 days, beginning at birth, and then removed abruptly.

Fig. 16 shows the model response to a 15% increase in the maximal oxygen consumption rate. Capillary growth is slightly accelerated at birth and less significantly retarded than normal with exposure to supplemental oxygen. Af-

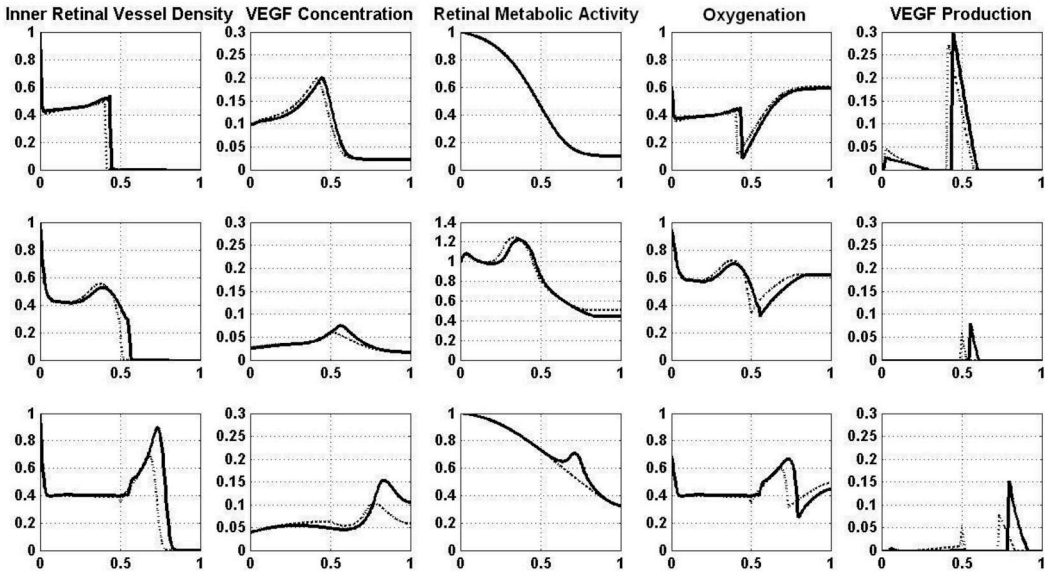

Fig. 16. Simulation results before and after 4 $\frac{1}{2}$ weeks of oxygen exposure in an infant with high retinal metabolism ($1.15B$). (Top) 24 weeks, at birth. (Middle) After 33 days of supplemental oxygen (28 $\frac{1}{2}$ weeks). (Bottom) after seven subsequent weeks of normal respiration (35 $\frac{1}{2}$ weeks). The dark and light curves correspond to elevated and normal B, respectively, under the same oxygen conditions

ter seven weeks of normal respiration, high VEGF levels and a pronounced peak in capillary density are observed. This is due to the elevated oxygen demand from differentiated retinal cells. This result suggests that a high maximal retinal metabolic rate might increase susceptibility to ROP.

Fig 17 shows the model response to a 15% decrease in the maximal oxygen consumption rate. Capillary growth is slightly slow at birth and more retarded than normal with exposure to supplemental oxygen. After seven weeks of normal respiration, capillary growth does not peak, but maintains a steady level. This is due to the lower oxygen demand from differentiated cells, which results in less VEGF production under hypoxic conditions. This suggests that a reduced maximal retinal metabolic rate might decrease susceptibility to ROP.

4.4 Model-Based Feedback Regulation of Oxygen Delivery

Variations in patient susceptibility to ROP make it unlikely that a single open-loop protocol can optimize systemic oxygenation and minimize the risk of ROP for all infants. However, we reason that some open-loop adjustments to current oxygen-delivery practices might provide more favorable conditions. For example, rather than abruptly withdrawing supplemental oxyen, we test whether gradual oxygen withdrawal might mitigate the development of ROP. Fig. 18 shows this alternative oxygen delivery system, where supplemental

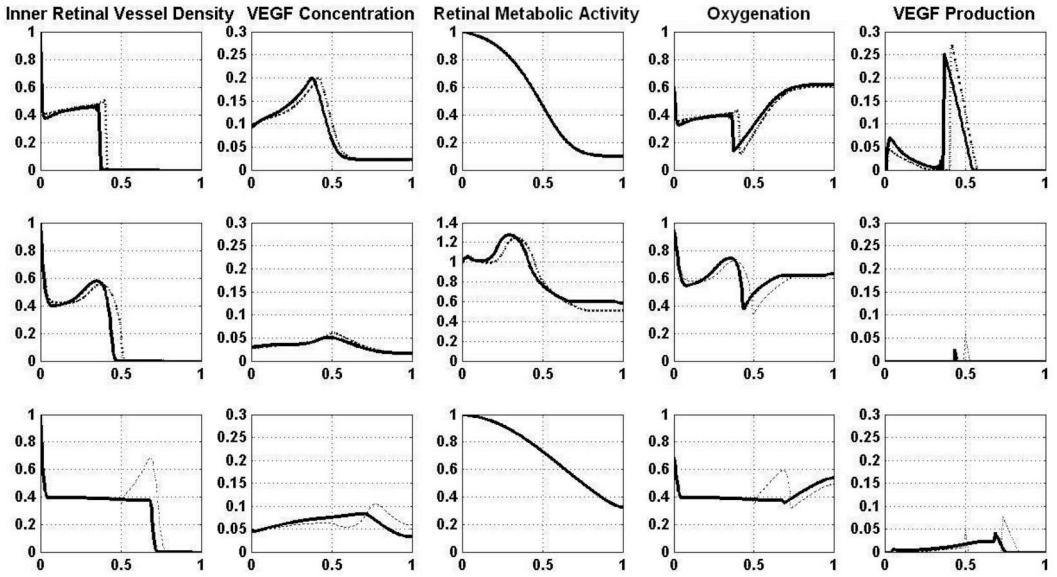

Fig. 17. Simulation results before and after 4 $\frac{1}{2}$ weeks of oxygen exposure in an infant with reduced retinal metabolism ($0.85B$). (Top) 24 weeks, at birth. (Middle) After 33 days of supplemental oxygen (28 $\frac{1}{2}$ weeks). (Bottom) after seven subsequent weeks of normal respiration (35 $\frac{1}{2}$ weeks). The dark and light curves correspond to reduced and normal B, respectively, under the same oxygen conditions.

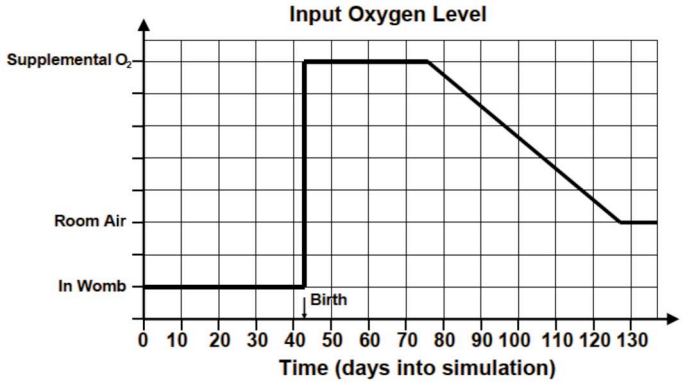

Fig. 18. Schematic for the gradual reduction of supplemental oxygen delivery.

oxygen is delivered for five weeks, then gradually reduced over 7 weeks. The following simulations assume preterm birth at 24 weeks; model parameters remain at values that reflect normal genetics.

Fig. 19 shows the model response to gradual (dark lines) and abrupt (light lines) withdrawal of supplemental oxygen. In both cases, after 5 weeks of supplemental oxygen, capillary growth pauses in response to hyperoxia (top row), as expected. However, $4\frac{1}{2}$ weeks later, the gradual transition to room air clearly suppresses the exaggerated peak in capillary density observed after abrupt oxygen withdrawal (middle row). Finally, after reaching ambient oxygen levels (bottom row), capillary growth remains stable with gradual oxygen withdrawal, but the capillary peak persists with abrupt oxygen withdrawal.

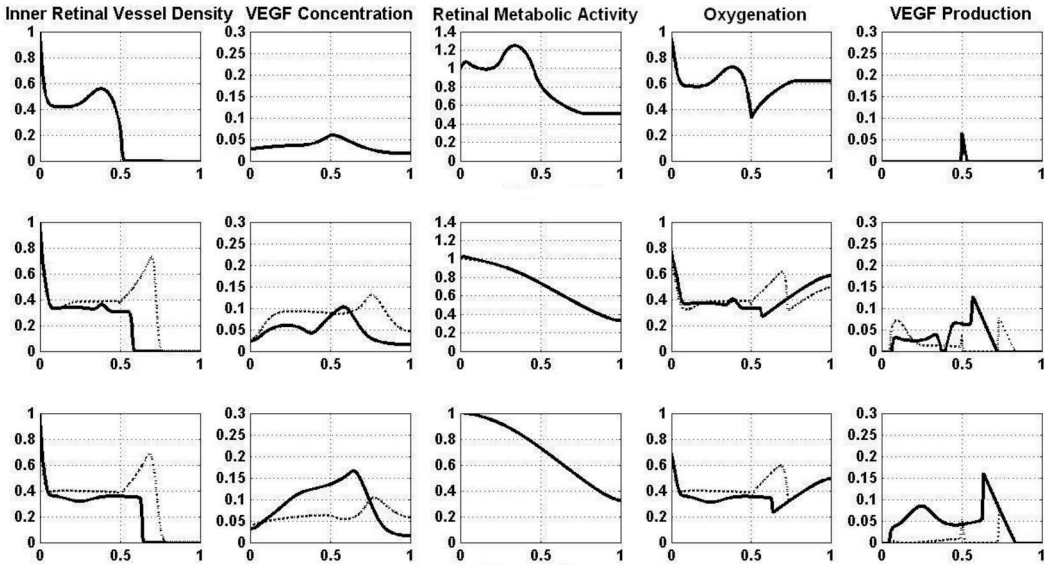

Fig. 19. Simulation results for the gradual reduction of supplemental oxygen. (Top) After birth (24 weeks) plus 5 weeks of supplemental oxygen. (Middle) Four and a half weeks after oxygen curtailment. (Bottom) Twelve weeks after birth; supplemental oxygen completely withdrawn. Dark and light curves correspond to gradual and abrupt oxygen curtailment, respectively.

These results suggest that gradual oxygen withdrawal may be an effective method for reducing the occurrence of ROP in premature infants that require supplemental oxygen.

5 Discussion

The model presented in this paper reproduces several key features of the natural and pathologic progression of retinal development. As retinal metabolic activity increases in the model, the oxygenation level in the retina drops, establishing the condition of physiological hypoxia considered to be the driving factor for the development of the inner retinal vasculature [Chan-Ling and Stone, 1993]. Model vessel density increases according to gradients of VEGF produced by hypoxic retinal cells in a manner evocative of experimental observations [Provis, 2001; Stone et al., 1995]. The model's peak vessel density at the front of the developing vasculature is followed by regions of lower vessel density nearer the optic disc, consistent with the documented over-proliferation and pruning of capillary sprouts [Hughes et al., 2000; Benjamin et al., 1998]. After 36 weeks of simulated development, model vessel density stops short of the ora serrata, consistent with the description of the "avascular zone" [Hughes et al., 2000].

Our ultimate goal is to provide guidelines for clinical oxygen delivery to avert

the emergence and progression of ROP. To that end, we've tested whether the model behaves in a manner consistent with clinical observations under conditions thought to influence the development of the disease. When the model's oxygenation level in the retinal circulation is set abnormally high, the density of retinal cells increases, and the subsequent reduction in VEGF secretion leads to a marked "pause" in the growth of retinal vessels. These observations are consistent with the formation of a cellular "ridge" between vascular and avascular retinal areas, considered the first known clinical indications of ROP [Phelps, 2001; Hutcheson, 2003]. When the model's oxygenation level in the retinal circulation is returned to a normal level, aggressive vessel growth ensues, consistent with the excessive capillary growth observed in ROP. The model predicts that excessive vascular growth will increase as the hyperoxia time increases. This suggests that a shorter incubation period in the NICU might reduce the progression of ROP. Additional simulations suggest that susceptibility to ROP might be reduced with interventions that lower maximal retinal oxygen consumption rates or slow capillary growth in response to VEGF. Finally, the model predicts that a very gradual withdrawal of oxygen supplementation can reduce or prevent the occurrence of ROP.

The results of the exploratory simulations herein should be interpreted with caution, because several physiological parameters are not available in the literature. In particular, the degree of susceptibility to ROP may be overestimated due to uncertainty in the fraction of endothelial cells converted to retinal cells. The fraction of capillary cells that convert to retinal cells is based on *in vitro* experimental conditions, and C_{cr} is chosen relative to the estimated value for normal behavior. Moreover, the model assumes that various parameters remain the same under altered genetic conditions, potentially leading to overestimates in retinal metabolic activity.

6 Conclusions and Future Work

A thorough understanding of the physiology underpinning ROP will enable the development of patient-specific closed-loop protocols whereby oxygen can be delivered in a time-varying fashion based on clinical observations of retinal vascular development and other appropriate biomarkers. In the future, we intend to develop candidate protocols of this kind with our model, applying formalized tools from feedback control theory.

The model presented in this paper is able to mimic many characteristics of the normal development of the inner retinal vasculature, and provides a good starting point for investigating the causes of ROP and potential treatment plans. A more detailed model is necessary, however, to capture all of the phenomena involved in the disease. For example, future models may address the

effects of vessel maturation on the development of the inner retinal capillary plexus and the dynamics of oxygen unloading from hemoglobin in the blood. This will allow better representations of genetic and environmental variability. Future models may also address the dependence of retinal cell differentiation on oxygen levels. This would introduce a function for cell death at low oxygen levels. In addition, new parameters should represent the distinction between healthy and damaged capillaries to improve the simulation of capillary competency for oxygen delivery. These modifications, along with more complete clinical data, will improve the fidelity of the model's behavior under conditions of supplemental oxygen.

In the future, we plan to refine our model based on experimental data to allow more quantitative predictions of the probability of developing ROP under different conditions. This will include representations of the different stages of ROP, and afford more variability in the representation of different neonatal conditions. Additionally, more complete representations of the retinal geometry will be implemented, accommodating radially asymmetric development and improving our ability to relate model behavior to the clinical stages of ROP. Finally, future models will incorporate more accurate estimates of parameters as future experimental research achieves the identification of surrogate markers measured in premature infants in the NICU. These refinements will provide more confidence in model predictions, and as the model becomes more quantitative, it may be used in sensitivity analyses to identify candidate molecular targets that can be tested experimentally.

References

Anderson, A., Chaplain, M., 1998. Continuous and discrete mathematical models of tumor-induced angiogenesis. Bulletin of Mathematical Biology 60, 857–899.

Askie, L., Henderson-Smart, D., 2001. Early versus late discontinuation of oxygen in preterm or low birth weight infants. Cochrane Database of Systematic Reviews 4.

Banin, E., Dorrell, M., Aguilar, E., Ritter, M., Aderman, C., Smith, A., Friedlander, J., Friedlander, M., 2006. T2-TrpRS inhibits preretinal neovascularization and enhances physiological vascular regrowth in OIR as assessed by a new method of quantification. Investigative Ophthalmology and Visual Science 47 (5), 2125–2134.

Beard, D., Bassingthwaighte, J., 2001. Modelling advection and diffusion of oxygen in complex vascular networks. Annals of Biomedical Engineering 29, 298–310.

Benjamin, L., Hemo, I., Keshet, E., 1998. A plasticity window for blood vessel remodelling is defined by pericyte coverage of the preformed endothelial

network and is regulated by PDGF-B and VEGF. Development 125, 1591–1598.

Bergers, G., Song, S., 2005. The role of pericytes in blood-vessel formation and maintenance. Neuro-Oncology 7, 452–464.

Chan-Ling, T., Stone, J., 1993. Retinopathy of prematurity: Its origins in the architecture of the retina. Progress in Retinal and Eye Research 12, 155–178.

Chaplain, M., Anderson, A., 1997. Mathematical modelling, simulation and prediction of tumor-induced angiogenesis. Invasion and Metastases 16, 222–234.

Chow, L., Wright, K., Sola, A., 2003. Can changes in clinical practice decrease the incidence of severe retinopathy of prematurity in very low birth weight infants? Pediatrics 111, 339–345.

Cringle, S., Yu, D., 2001. Oxygen distribution and consumption within the retina in vascularised and avascular retinas and in animal models of retinal disease. Progress in Retinal and Eye Research 20, 175–208.

Cryotherapy for Retinopathy of Prematurity Cooperative Group, 2001. Multicenter trial of cryotherapy for retinopathy of prematurity: Ophthalmological outcomes at 10 years. Archives of Ophthalmology 119, 1110–1118.

Deissler, H., Deissler, H., Lang, G., Lang, G., 2006. TGFβ induces transdifferentiation of iBREC to αSMA-expressing cells. International Journal of Molecular Medicine 18, 577–582.

Dor, Y., Porrat, R., Keshet, E., 2001. Vascular endothelial growth factor and vascular adjustments to perturbations in oxygen homeostasis. American Journal of Physiology: Cell Physiology 280, C1367–C1374.

Drake, C., Little, C., 1995. Exogenous vascular endothelial growth factor induces malformed and hyperfused vessels during embryonic neovascularization. Proceedings of the National Academy of Sciences of the United States of America 92, 7657–7661.

Ferrara, N., 2001. Role of vascular endothelial growth factor in regulation of physiological angiogenesis. American Journal of Physiology: Cell Physiology 280, C1358–C1366.

Foos, R., 1988. Pathologic features of retinopathy of prematurity. In: Flynn, J. T., Phelps, D. L. (Eds.), Retinopathy of Prematurity: Problem and Challenge. Alan R. Liss, Inc., pp. 73–85.

Galluzzi, P., Venturi, C., Cerase, A., Vallone, I., Bracco, S., Bardelli, A., Hadjistilianou, T., Gennari, P., Monti, L., Filosomi, G., 2001. Coats disease: Smaller volume of the affected globe. Progress in Retinal and Eye Research 221, 64–9.

Gariano, R., 2001. Cellular mechanisms in retinal vascular development. Progress in Retinal and Eye Research 22, 295–306.

Garner, A., 1985. The pathology of retinopathy of prematurity. In: Silverman, W. A., Flynn, J. T. (Eds.), Retinopathy of Prematurity. Blackwell Scientific Publications, pp. 19–52.

Gazit, Y., Berk, D. A., Leunig, M., Baxter, L. T., Jain, R. K., 1995. Scale-invariant behavior and vascular network formation in normal and tumor

tissue. Physical Review Letters 75, 2428–2431.

Gerhardt, H., Golding, M., Fruttiger, M., Ruhrberg, C., Lundkvist, A., Abramsson, A., Jeltsch, M., Mitchell, C., Alitalo, K., Shima, D., Betsholtz, C., 2003. VEGF guides angiogenic sprouting utilizing endothelial tip cell filopodia. Journal of Cell Biology 161, 1163–1177.

Glass, P., 1998. Light toxicity in developing retinal vasculature. In: Flynn, J., Phelps, D. (Eds.), Retinopathy of Prematurity: Problem and Challenge. Alan R. Liss, Inc., pp. 103–117.

Hernandez-Sanchez, C., Lopez-Carranza, A., Alarcon, C., de La Rosa, E., de Pablo, F., 1995. Autocrine/paracrine role of insulin-related growth factors in neurogenesis: Local expression and effects on cell proliferation and differentiation in retina. Proceedings of the National Academy of Sciences of the United States of America 92, 9834–8.

Hughes, S., Yang, H., Chan-Ling, T., 2000. Vascularization of the human fetal retina: Roles of vasculogenesis and angiogenesis. Investigative Ophathalomolgy and Visual Science 41, 1217–1228.

Hutcheson, K., 2003. Retinopathy of prematurity. Current Opinions in Ophthalomology 14, 286–290.

Institute, N. E., 2004. Retinopathy of prematurity.
URL `http://www.nei.nih.gov/health/rop/index.asp`

Jakobiec, F., 1982. Ocular Anatomy Embryology and Teratology. Harper & Row.

Kaufman, P., Alm, A., 2003. Alder's Physiology of the Eye: Clinical Application, 10th Edition. Mosby.

Kavanagh, B., Secomb, T., Hsu, R., Lin, P., Venitz, J., Dewhirst, M., 2002. A theoretical model for the effects of reduced hemoglobin-oxygen affinity on tumor oxygenation. International Journal of Radiation Oncology, Biology, Physics 53, 172–179.

Kendall, R., Rutledge, R., Mao, X., Tebben, A., Hungate, R., Thomas, K., 1999. Vascular endothelial growth factor receptor KDR tyrosine kinase activity is increased by autophosphorylation of two activation loop tyrosine residues. The Journal of Biological Chemistry 274, 6453–6460.

Kolb, H., Fernandez, E., Nelson, R., 2003. Webvision: The organization of the retina and visual system.
URL `http://www.webvision.med.utah.edu`

Lashkari, K., Hirose, T., Yazdany, J., McMeel, J., Kazlauskas, A., Rahimi, N., 2000. Vascular endothelial growth factor and hepatocyte growth factor levels are differentially elevated in patients with advanced retinopathy of prematurity. American Journal of Pathology 156, 1337–1344.

Levine, H., Sleeman, B., Nilsen-Hamilton, M., 2000. A mathematical model for the roles of pericytes and macrophages in the initiation of angiogenesis. i. the role of protease inhibitors in preventing angiogenesis. Mathematical Biosciences 168, 77–115.

Levine, H., Sleeman, B., Nilsen-Hamilton, M., 2001. Mathematical modeling of the onset of capillary formation initiating angiogenesis. Journal of Math-

ematical Biology 42, 195–238.

Maggelakis, S., Savakis, A., 1996. A mathematical model of growth factor induced capillary growth in the retina. Mathematical Computer Modelling 24, 33–41.

Maggelakis, S., Savakis, A., 1999. A mathematical model of retinal neovascularization. Mathematical and Computer Modelling 29, 91–97.

Mikaniki, E., Mikaniki, M., Shirzadian, A., 2012. Effects of blood transfusion on retinopathy of prematurity. In: Kochhar, P. (Ed.), Blood Transfusion in Clinical Practice.
URL `http://www.intechopen.com/books/blood-transfusion-in-clinical-practice/effects-of-blood-transfusion-on-retinopathy-of-prematurity`

Miquerol, L., Langille, B., Nagy, A., 2000. Embryonic development is disrupted by modest increases in vascular endothelial growth factor gene expression. Development 127, 3941–3946.

Niemisto, A., Dunmire, V., Yli-Harja, O., Zhang, W., Shmulevich, I., 2005. Analysis of angiogenesis using in vitro experiments and stochastic growth models. Physical Review E 72, 062902(1–4).

Phelps, D., 2001. Retinopathy of prematurity: History, classification, and pathophysiology. NeoReviews 2, ee153–ee166.

Provis, J., 2001. Development of the primate retinal vasculature. American Journal of Diseases of Children 20, 799–821.

Provis, J., Leech, J., Diaz, C., Penfold, P., Stone, J., Keshet, E., 1997. Development of the human retinal vasculature: Cellular relations and VEGF expression. Experimental Eye Research 65, 555–568.

Reynolds, J., 2001. The management of retinopathy of prematurity. Paediatric Drugs 3, 263–272.

Risau, W., 1997. Mechanisms of angiogenesis. Nature 386, 671–674.

Rodieck, R., 1998. The First Steps in Seeing. Sinauer Associates, Inc.

Sapieha, P., Joyal, J., Rivera, J., Kermorvant-Duchemin, E., Sennlaub, F., Hardy, P., Lachapelle, P., Chemtob, S., 2010. Retinopathy of prematurity: Understanding ischemic retinal vasculopathies at an extreme of life. Journal of Clinical Investigation 120, 3022–3032.

Shima, D., Adamis, A., Ferrara, N., Yeo, K., Yeo, T., Allende, R., Folkman, J., D'Amore, P., 1995. Hypoxic induction of endothelial cell growth factors in retinal cells: Identification and characterization of vascular endothelial growth factor (VEGF) as the mitogen. Molecular Medicine 1, 182–193.

Sinha, S., Tin, W., 2003. The controversies surrounding oxygen therapy in neonatal intensive care units. Current Opinions in Pediatrics 15, 161–165.

Sonmez, K., Drenser, K., Jr., A. C., Trese, M., 2008. Vitreous levels of stromal cell-derived factor 1 and vascular endothelial growth factor in patients with retinopathy of prematurity. Ophthalmology 115, 1065–1070.

Stokes, C. L., Lauffenburger, D. A., 1991. Analysis of the roles of microvessel endothelial cell random motility and chemotaxis in angiogenesis. Journal of Theoretical Biology 152, 377–403.

Stone, J., Itin, A., Alon, T., Pe'er, J., Gnessin, H., Chan-Ling, T., Keshet, E., 1995. Development of retinal vasculature is mediated by hypoxia-induced vascular endothelial growth factor (VEGF) expression by neuroglia. The Journal of Neuroscience 15, 4738–4747.

Sun, Y., Dalal, R., Gariano, R., 2010. Cellular composition of the ridge in retinopathy of prematurity. Archives of Ophthalmology 128 (5), 638–641.

The STOP-ROP Multicenter Study Group, 2000. Supplemental therapeutic oxygen for prethreshold retinopathy of prematurity (STOP-ROP), a randomized, controlled trial. I: Primary outcomes. Pediatrics 105, 295–310.

Tin, W., Milligan, D., Pennefather, P., Hey, E., 2002. Pulse oximetry, severe retinopathy, and outcome at one year in babies of less than 28 weeks gestation. Archives of Disease in Childhood. Fetal and Neonatal Edition 84, 361–367.

Tong, S., Yuan, F., 2001. Numerical simulations of angiogenesis in the cornea. Microvascular Research 61, 14–27.

Vaughn, D., Asbury, T., Riordan-Eva, P., 1999. General Ophthalmology. Appelton & Lange.

Waltenberger, J., Claesson-Welsh, L., Siegbahn, A., Shibuya, M., Heldin, C., 1994. Different signal transduction properties of KDR and Flt1, two receptors for vascular endothelial growth factor. The Journal of Biological Chemistry 269, 26988–26995.

Wang, D., Lehman, R., Donner, D., Matli, M., Warren, R., Welton, M., 2002. Expression and endocytosis of VEGF and its receptors in human colonic vascular endothelial cells. American Journal of Physiology. Gastrointestinal and Liver Physiology 282, G1088–G1096.

Yu, D.-Y., Cringle, S. J., 2001. Oxygen distribution and consumption within the retina in vascularised and avascular retinas and in animal models of retinal disease. Progress in Retinal and Eye Research 20, 175–208.

Zhang, W., Yokota, H., Xu, Z., Narayanan, S., Yancey, L., Yoshida, A., Marcus, D., Caldwell, R., Caldwell, R., Brooks, S., 2011. Hyperoxia therapy of pre-proliferative ischemic retinopathy in a mouse model. Investigative Ophthalmology and Visual Science 52 (9), 6384–6395.